B and Li distribution in the Peña Negra complex: An alpha-track study

M. Dolores Pereira[1] and Denis M. Shaw[2]

[1]Departamento de Geología, Facultad de Ciencias, Universidad de Salamanca, 37008 Salamanca, Spain
[2]Department of Geology, McMaster University, Hamilton, Ontario L8S 4M1, Canada

Abstract

Alpha-track imaging (ATI) provides a map of the surface distribution of B + Li across a polished thin section and can reveal textural detail that is otherwise not accessible. It is also useful for studying minerals such as cordierite, which can be difficult to distinguish.

In minerals from the Peña Negra anatectic complex, Spain, the image density decreases in the order tourmaline $\gg$ sillimanite $\approx$ muscovite $\approx$ sericite > chlorite > cordierite > biotite > feldspar $\approx$ quartz. The sillimanite image comes mostly from B, the cordierite and biotite images reflect the content of Li, and muscovite and sericite contain both.

The Peña Negra rocks contain less B and Li than many European Hercynian granitic complexes, and the anatectic process retained these elements in the restites rather than concentrating them in the granitic melt.

Introduction

Modern techniques, such as the electron microprobe, cathodoluminescence, and Normarski contrast interference, have complemented standard petrographic methods. The present paper draws attention to the alpha-track image (ATI), which uses B and Li distributions to delineate textural features in metamorphic rocks, as another useful aid.

Use of the ATI was pioneered by Armijo and Rosenbaum (1967), Seitz (1973), Seitz and Hart (1973), and Kleeman (1973) following extensive work on various track detectors by R.L. Fleischer and collaborators (e.g., Fleischer et al. 1967). Its use is limited only by the difficulty of obtaining access to irradiation facilities. Recent applications include studies of igneous, metamorphic, and lunar rocks by Ahmad and Wilson (1981), Truscott and Shaw (1984), Truscott et al. (1986), Shaw (1995), Shaw et al. (1988a, 1988b), Sauerer et al. (1989), Leeman et al. (1992), and Moran et al. (1992) but not yet migmatitic rocks.

In this article we show how the ATI may help in regional studies of granitic migmatite terranes, citing the Peña Negra anatectic complex in central Spain as an example (Pereira 1989, 1992; Bea and Pereira 1990). Concentrations of B and Li in granitic complexes vary widely, and the Peña Negra is relatively impoverished in these elements.

Analytical methods

Following the methods of Fleischer et al. (1975), Truscott and Shaw (1984), and Shaw et al. (1988b), polished thin sections from samples collected in the anatectic complex and detector film were irradiated at McMaster University, with a neutron flux of 6×10^7 (cm^{-2}s^{-1}). The films were then etched to reveal the areas damaged by alpha particles from the reactions $^{10}B + n = ^7Li + \alpha$ and

$^6Li + n = ^3H + \alpha$. The detector images, at high magnification, consist of alpha tracks, each about 0.4×0.7 μm; under low magnification, the tracks merge and give an image of each mineral grain. The track density is proportional to the abundance of B, Li, or both (hereafter indicated as B + Li) at the surface of the sample. The detectors were photographed and used as negative prints. Attempts to distinguish the effects of B from those of Li were unsuccessful, although their alphas have different energies. For minerals containing both elements at the same concentrations, the track density from B is 10–15 times stronger than from Li, assuming terrestrial isotopic ratios, because of the higher neutron-capture cross section of B.

Quantitative analyses of B and Li were made using laser-ablation, inductively coupled plasma mass spectrometry (LA-ICP-MS) with a Perkin-Elmer model 302 laser-ablation system coupled to a PE SCIEX ICP-MS Elan-5000 spectrometer. Craters produced were about 40–80 μm in diameter and 10–40 μm in depth. Estimated relative standard deviations for concentrations of 50, 10, and 1 ppm are ±5, ±10, and $\pm25\%$, respectively. The minerals analyzed were cordierite, biotite, sillimanite, muscovite, potassium feldspar, and plagioclase. Data from these analyses are compared to the qualitative results obtained from alpha-particle mapping.

B analysis of bulk samples utilized prompt-gamma neutron activation analysis in the nuclear reactor of McMaster University (Higgins et al. 1984). Li contents in whole-rock samples were analyzed by ICP-MS.

Samples

The protolith of the migmatites of the Peña Negra complex consists of metasediments and orthogneisses. These rocks underwent low-pressure metamorphism followed by anatexis during the Hercynian orogeny; partial

TABLE 1. Concentrations of B and Li in the main rock types of the Peña Negra anatectic complex

Lithotype	n	B (ppm)		Li (ppm)	
		Avg.	Range	Avg.	Range
Migmatite	16	20	4–124	65	39–138
Leucogranite	11	15	4–47	39	15–118
Restite	3	45	9–104	152	135–181

melting produced granitic and granodioritic melt segregates, leaving residual migmatites or restites, as described in detail in Pereira (1989), Bea and Pereira (1990), and Pereira and Bea (1994). Eighty-three samples were taken for petrographic, major, and trace element analysis, and a small number were used for alpha-track studies. The concentrations of B and Li in the main rock types are shown in Table 1; although only a few rocks could be grouped exclusively as restite, similar melanocratic assemblages occur among the migmatites. Four examples were chosen to illustrate the use of the method.
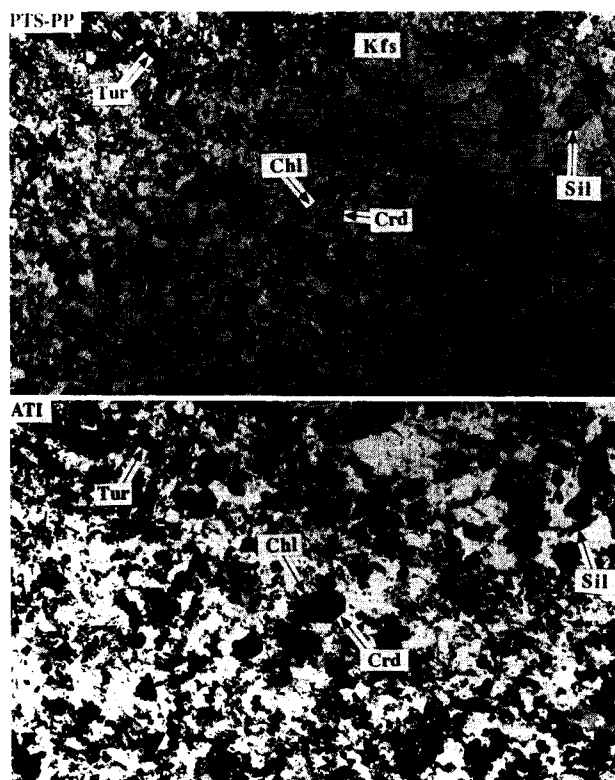

FIGURE 1. Restite (GREB-370) consisting largely of cordierite (Crd), sillimanite (Sil), and biotite with minor amounts of ilmenite and quartz and a few grains of potassium feldspar (Kfs). The darkest ATI is produced by the fresh crystals of cordierite, surrounded by lighter areas produced by chlorite (Chl). Sillimanite gives an image almost as dark as cordierite, but biotite is lighter. Ilmenite, quartz, and feldspar generate no image. The tourmaline (Tur) image can scarcely be distinguished from the one given by sillimanite. The rock contains 104 ppm B and 78 ppm Li. **Top:** PP, plane-polarized light; **bottom:** ATI, alpha-track image. Field of view ≈ 30 × 18 mm.
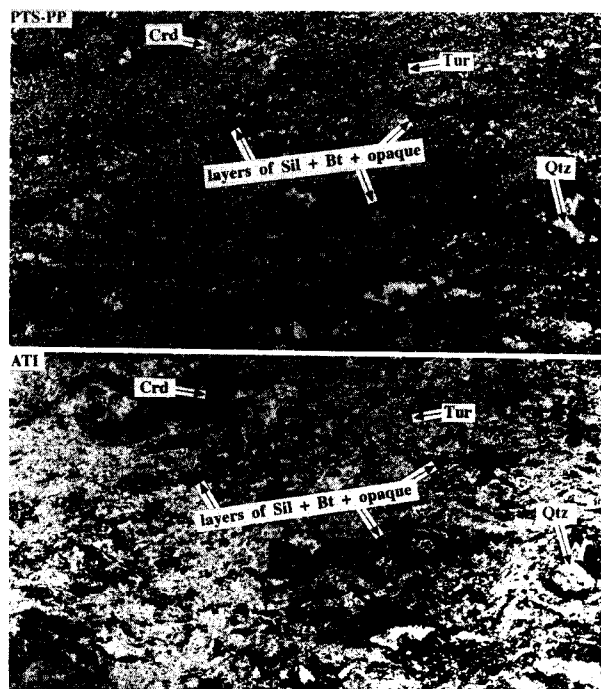

FIGURE 2. Restitic melanosome (GREB-607) of migmatite consisting of layers of biotite (Bt) + sillimanite + ilmenite, surrounding grains of pinitized cordierite and aggregates of quartz (Qtz). In the ATI, the rock fabric is very clear and the dark layers are made up of tracks produced by B in sillimanite and Li in biotite. The dark cordierite image is due to B and Li in pinite. Quartz and ilmenite produce no image. Tourmaline forms small round grains. The rock has 66 ppm B and 75 ppm Li. Abbreviations and field of view as in Figure 1.

FEATURES OF ALPHA-TRACK IMAGES IN PEÑA NEGRA ROCKS

As negative images, the darkest areas on Figures 1–4 correspond to the highest concentrations of B + Li. The ATIs are most conveniently studied with the optical plane-polarized (PP) or cross-polarized (CP) images either using two microscopes side by side or by mounting photographs as in Figures 1–4. The amount of detail in an ATI depends on skillful processing of the photographic image, which usually yields better results than visual observation on the microscope stage. The value of an ATI is twofold: First, it provides supplementary textural information, and, second, it maps the distribution of B + Li.

The rocks depicted in Figures 1 and 2 are typical of the residues from an episode of rock melting in the Peña Negra complex, which produced veins and sheets of granodiorite and granite (see Fig. 3). The first, sample GREB-370 in Figure 1, consists largely of cordierite, sillimanite, and biotite with minor amounts of ilmenite and quartz, and a few grains of potassium feldspar; a few minute grains of tourmaline are present. The fabric is granular and massive; cordierite is subhedral, and this texture is clearly visible only in the ATI.
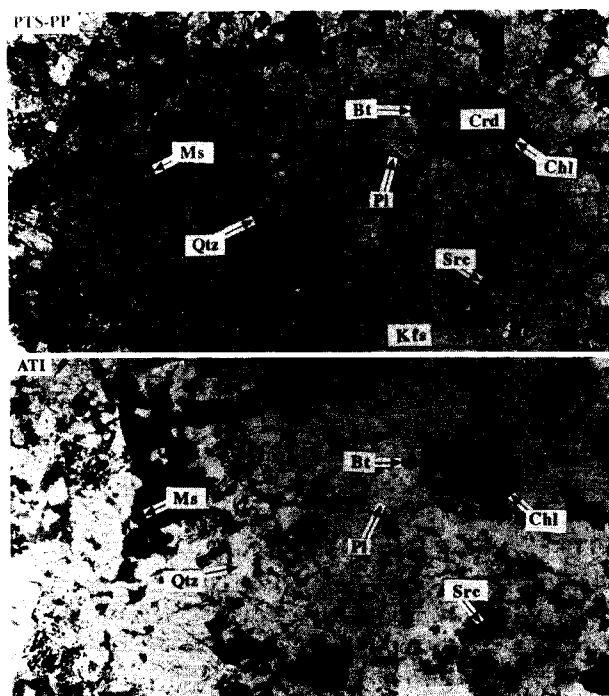
FIGURE 3. Cordierite leucogranite (GRELO-33). Cordierite and biotite are the only mafic minerals in this rock. The darkest images are from muscovite (Ms) and chlorite, which are both derived from the alteration of cordierite, and from sericite (Src), which is derived from the alteration of feldspar. The subhedral pinitized cordierite gives a lighter image than when it is fresh (compare with Fig. 1). Quartz, plagioclase (Pl), and potassium feldspar form no images. The rock abundances of B and Li are 26 and 46 ppm, respectively. Abbreviations and field of view as in Figures 1 and 2.

FIGURE 4. Migmatite (GRELO-2) affected by a shear zone, which is seen as the dark area of altered sillimanite and cordierite. The areas of low track density are produced by opaques, feldspar, and quartz but also include sericitized feldspar with some sillimanite and cordierite. Abbreviations and field of view as in Figure 1.

The other sample (GREB-607 in Fig. 2) is quite different. It is a deformed migmatite melanosome representative of the residues from melting, and, although it is similarly composed of biotite, sillimanite, and ilmenite, which surround grains of pinitized cordierite and aggregates of quartz, the fabric is different. The ATI is particularly useful for this rock because it shows the augen texture and the rolled and fragmented nature of the cordierite much more clearly than the optical image; it is also evident that the ATI would be better than the optical image for estimating the modal proportion of cordierite. Tourmaline is again present as a very minor accessory.

A cordierite leucogranite (GRELO-33) is shown in Figure 3. The subhedral cordierite is pinitized and locally altered to chlorite and muscovite; its modal abundance also can be more readily measured on the ATI. It may be noted that a strong alpha image is shown by the sericitic alteration of the feldspar.

A migmatite traversed by a zone of deformation is seen in Figure 4. Within the sheared area is a concentration of sillimanite, completely sericitized, and cordierite, completely pinitized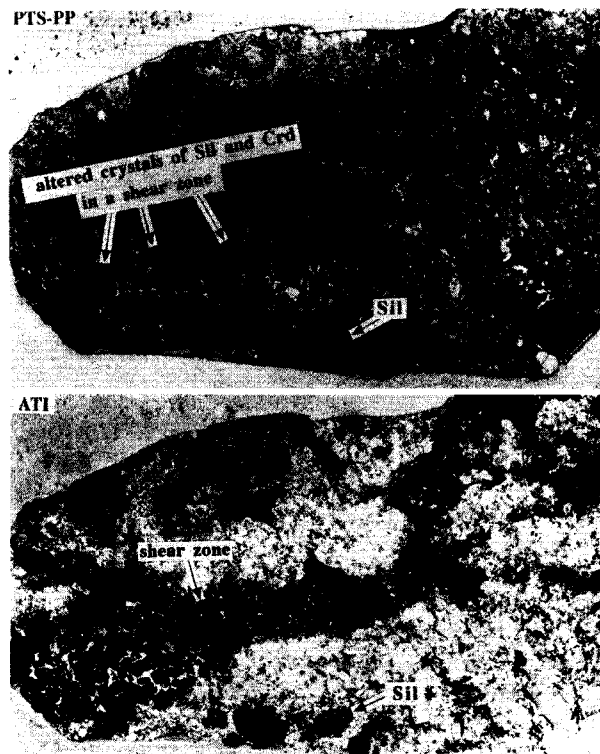; it is these micaceous alteration products that generate the strong contrasts in the ATI, contrasts that are not clearly visible in the PP photomicrographs.

NOTES ON THE MINERALS

The alpha images of the constituent minerals in Figures 1–3 correspond to the following decreasing intensity order: tourmaline $\gg$ sillimanite $\approx$ muscovite $\approx$ sericite > chlorite > cordierite > biotite > feldspar $\approx$ quartz. Actually, the position of cordierite in this sequence depends on its extent of alteration (see later).

B and Li may occur in rocks in the following ways: (1) by incorporation in minerals during crystallization, isomorphically substituting for major elements; e.g., Si^{4+} and Al^{3+} in the case of B^{3+}, and Mg^{2+} and Fe^{2+} in the case of Li^+ (Malinko et al. 1979); (2) as inclusions, both solid and fluid, in minerals; e.g., see Roedder (1984), London et al. (1987); and (3) by adsorption along grain boundaries, fractures, phyllosilicate interlayers, etc., from fluid deposition; e.g., see Ahmad and Wilson (1981), Sauerer et al. (1989). The measured abundances in the Peña Negra minerals are shown in Table 2.

Tourmaline was initially overlooked. However, yellow images, where the alpha tracks were so intense that they

TABLE 2. Concentrations of B and Li in the Peña Negra minerals

Mineral	n	B (ppm) Avg.	B (ppm) Range	Li (ppm) Avg.	Li (ppm) Range
Cordierite	7	5	0.3–19	441	454–465
Sillimanite	7	15	7–27	n.d.	
Muscovite	8	15	0.2–34		
Biotite	3	7	1–12	151	110–166
Potassium feldspar	2	2		6	5–8
Plagioclase	6	5	0.7–7	3	1–4

Note: These analyses from Bea et al. (1994) and F. Bea personal communication; n.d. = below detection limit.

saturated or burned the detector (Seitz and Hart 1973), indicated high B + Li, and tourmaline was then recognized visually as minute grains (~0.5 μm) in some restites and melanosomes.

Both fresh and altered cordierite produce high-density alpha-track images: (1) fresh cordierite gives a darker image than surrounding chlorite and biotite; (2) in altered cordierite the pinite produces a lighter image than nearby muscovite, biotite, and chlorite. The ATI for fresh cordierite is caused by the high content of Li and not by B; this is clear from the Peña Negra data in Table 2, which are from LA-ICP-MS analyses on fresh grains and indicate abundant Li and low B. Grew et al. (1987) similarly recorded ion probe measurements of 98 ppm Li and no detectable B in a fresh cordierite, although elsewhere reported (Grew et al. 1991) a Russian cordierite containing 9 ppm Li and 19 ppm B. Analyses of cordierite separates for trace elements may be misleading because of inclusions; but Armbruster and Irouschek (1983) analyzed cordierite separates as fresh as possible, and their atomic absorption results for Li (100–450 ppm) seem reliable because the content was higher in fresh (where it substitutes for Mg^{2+}) than in altered cordierite. In addition, cordierite containing a high number of channel cations, notably Na^+, as in this complex (Pereira and Bea 1994), is known to be enriched in Li (Grew et al. 1990).

Sillimanite is very variable in reported B content, although its Li content is negligible (Grew et al. 1990). Thus, Grew and Hinthorne (1983) found high contents of B, averaging 932 ppm, in six samples of sillimanite from B- and F-rich granulites. The Peña Negra sillimanite does not show high B content (Table 2), although sufficient to account for its alpha-track image. It is slightly nonstoichiometric with a deficit of Al (Pereira 1992), which was thought to be compensated by the (sometimes) high content of Ti and Fe (Kerrick 1990; Grew and Rossman 1985), but there is not sufficient B to explain the deficit by substitution of B for Si. The high B concentrations in various sillimanite samples reported by Pearson and Shaw (1960) are probably due to muscovite impurities.

Muscovite, sericite, and chlorite give intense alpha-track images. Muscovite contains 20–600 ppm B (Harder 1969; Bebout et al. 1992) and up to 1.67 wt% Li (Deer et al. 1992). Chlorite can accumulate up to 50 ppm B (Harder

1969). Biotite generates a weaker image than these minerals; it contains negligible B (see, e.g., Jones and Smith 1984; Grew et al. 1990) but substantial Li (see Table 2).

Shearer and Papike (1986) and Sauerer et al. (1989) claimed a moderate content of B in feldspars, but this is not common (Malinko et al. 1979) unless the feldspars are sericitized. Quartz commonly shows traces of B and Li, which may reflect lattice substitution or mineral inclusions [e.g., Hervig and Peacock (1989) report ~20 ppm Li and ~1.5 ppm B in quartz from a mylonitic zone]. Quartz and feldspars from the Peña Negra have such low contents (Table 2) that they generate no images except from sericitic alteration.

Oxides and other accessory minerals, which include apatite, ilmenite, zircon, pyrite, graphite, monazite, and xenotime do not generate any alpha tracks, with the exception of course of tourmaline.

INTERPRETATIONS

In the course of metamorphism, B and Li are commonly lost at higher grades, partially by release during breakdown of sericite, muscovite, and biotite, and partially because their breakdown products are soluble in fluids that are also released; tourmaline, however, usually resists breakdown until granulite facies conditions are obtained (Werding and Schreyer 1984).

It has already been noted that the restites contain a little visible tourmaline. Table 1 shows that, although variable in B content, both the restites and the migmatite group contain more B and Li than the leucogranites. As mentioned earlier, the migmatite group includes residual or restitic materials (such as the melanosome GREB-607 in Fig. 2).

It thus appears that B + Li loss did not occur during this anatexis; the residues from melting retained a substantial part, the B being held in tourmaline, and the leucogranite melts were depleted in both B and Li. This contrasts sharply with many Hercynian granitic complexes elsewhere in Europe, which are strongly enriched in these elements (e.g., Sauerer and Troll 1990; Exley et al. 1983).

REFERENCES CITED

Ahmad, R., and Wilson, C.J.L. (1981) Uranium and boron distributions related to metamorphic microstructure: Evidence for metamorphic fluid activity. Contributions to Mineralogy and Petrology, 76, 24–32.
Armbruster, T., and Irouschek, A. (1983) Cordierites from the Lepontine Alps: Na + B Al substitution, gas content, cell parameters and optics. Contributions to Mineralogy and Petrology, 82, 389–396.

Armijo, J.S., and Rosenbaum, H.S. (1967) Boron detection in metals by alpha-particle tracking. Journal of Applied Physics, 38, 2064–2069.

Bea, F., and Pereira, M.D. (1990) Estudio petrológico del complejo ana-téctico de la Peña Negra, batolito de Avila, España central. Revista de la Sociedad Geológica de España, 3, 87–104.

Bea, F., Pereira, M.D., and Stroh, A. (1994) Mineral/leucosome trace element partitioning in a peraluminous migmatite (a laser ablation-ICP-MS study): Constraints on melt-producing reactions and chemical fractionation during crustal anatexis. Chemical Geology, 117, 291–312.

Bebout, G.E., Graham, C.M., Leeman, W.P., and Sisson, V.B. (1992) Trace element distribution and mobility during prograde metamorphism of sediments: Ion-microprobe study of the Pelona Schist, California. Eos, 73, 327.

Deer, W.A., Howie, R.A., and Zussman, J. (1992) An introduction to the rock-forming minerals (2nd edition), 696 p. Longman, London.

Exley, C.S., Stone, M., and Floyd, P.A. (1983) Composition and petrogenesis of the Cornubian granite batholith and post-orogenic volcanic rocks in southwest England. In P.L. Hancock, Ed., The Variscan fold belt in the British Isles, p. 153–177. Adam Hilger, London.

Fleischer, R.L., Price, P.B., Walker, R.M., and Hubbard, E.L. (1967) Criterion for registration in dielectric track detectors. Physical Review, 156, 353–366.

Fleischer, R.L., Price, P.B., and Walker, R.M. (1975) Nuclear tracks in solids, p. 509–514. University of California Press, Berkeley.

Grew, E.S., and Hinthorne, J.R. (1983) Boron in sillimanite. Science, 221, 547–549.

Grew, E.S., and Rossman, G.R. (1985) Co-ordination of boron in sillimanite. Mineralogical Magazine, 49, 132–135.

Grew, E.S., Abraham, K., and Medenbach, O. (1987) Ti-poor hoegbomite in kornerupine-sillimanite rocks from Ellammankovilpatti, Tamil Nadu, India. Contributions to Mineralogy and Petrology, 95, 21–31.

Grew, E.S., Chernosky, J.V., Werding, G., Abraham, K., Marquez, N., and Hinthorne, J.R. (1990) Chemistry of kornerupine and associated minerals, a wet chemical, ion microprobe and X-ray study emphasizing Li, Be, B and F contents. Journal of Petrology, 31, 1025–1070.

Grew, E.S., Yates, M.G., Beryozkin, V.I., and Kitsul, V.I. (1991) Kornerupine in slyudites from the Usmun river basin on the Aldan Shield: II. Chemistry of the minerals, mineral reactions. Soviet Geology and Geophysics, 32, 66–74.

Harder, H. (1969) Boron content of sediments as a tool in facies analysis. Sedimentary Geology, 4, 153–175.

Hervig, R.L., and Peacock, S.M. (1989) Implications of trace element zoning in deformed quartz from the Santa Catalina mylonite zone. Journal of Geology, 89, 343–350.

Higgins, M.D., Truscott, M.G., Shaw, D.M., Bergeron, M., Buffet, G.H., Copley, J.R.D., and Prestwick, W.V. (1984) Prompt-gamma neutron activation analysis at McMaster Nuclear Reactor. Atomkern-energie Kerntechnik, 44, 690–697.

Jones, A.P., and Smith, J.V. (1984) Ion probe analysis of H, Li, B, F and Ba in micas, with additional data for metamorphic amphibole, scapolite and pyroxene. Neues Jahrbuch für Mineralogie Monatshefte, 5, 228–240.

Kerrick, D.M. (1990) The Al₂SiO₅ polymorphs. In Mineralogical Society of America Reviews in Mineralogy, 22, 406 p.

Kleeman, J.D. (1973) The role of lithium and boron in forming Lexan plastic prints. Geochimica et Cosmochimica Acta, 56, 775–788.

Leeman, W.P., Sisson, V.B., and Reid, M.R. (1992) Boron geochemistry of the lower crust: Evidence from granulite terranes and deep crustal xenoliths. Geochimica et Cosmochimica Acta, 56, 775–788.

London, D., Hervig, R.L., and Morgan, G.B., VI (1987) Melt-vapor solubilities and elemental partitioning in peraluminous granite-pegmatite systems: Experimental results with Macusani glass at 200 MPa. Contributions to Mineralogy and Petrology, 99, 360–373.

Malinko, S.V., Berman, J.B., Lisitsyn, A.Y., and Stoliarova, A.N. (1979) Boron in rock forming minerals based on data from a local radiographic analysis. International Geological Review, 21, 1274–1284.

Moran, A.E., Sisson, V.B., and Leeman, W.P. (1992) Boron depletion during progressive metamorphism: Implications for subduction processes. Earth and Planetary Science Letters, 111, 331–349.

Pearson, G.R., and Shaw, D.M. (1960) Trace elements in kyanite, sillimanite and andalusite. American Mineralogist, 45, 808–817.

Pereira, M.D. (1989) Migmatización diatexítica y la génesis de las granodioritas subautóctonas del Complejo Anatéctico de la Peña Negra, Batolito de Avila. M.Sc. thesis, Universidad de Salamanca, Salamanca, Spain.

———(1992) El complejo Anatéctico de la Peña Negra (Batolito de Avila): Un estudio de la anatexia cortical en condiciones de baja presión, 355 p. Ph.D. thesis, Universidad de Salamanca, Salamanca, Spain.

Pereira, M.D., and Bea, F. (1994) Cordierite-producing reactions at the Peña Negra Complex, Avila Batholith, central Spain: The key role of cordierite in low-pressure anatexis. Canadian Mineralogist, 32, 763–780.

Roedder, E. (1984) Fluid inclusions. In Mineralogical Society of America Reviews in Mineralogy, 12, 644 p.

Sauerer, A., Troll, G., and Matthies, D. (1989) Microdistribution of boron: Particle-track images from samples of a Caledonian igneous complex. Terra Nova, 1, 359–364.

Sauerer, A.F., and Troll, G. (1990) Abundance and distribution of boron in the Hauzenberg (Bavaria) granite complex. Geochimica et Cosmochimica Acta, 54, 49–56.

Seitz, M.G. (1973) Boron mapping and partitioning in synthetic and natural systems: Crystal-melt assemblages, garnet lherzolite, chondrites. Carnegie Institution of Washington Year Book, 72, 588–592.

Seitz, M.G., and Hart, S.R. (1973) Uranium and boron distributions in some oceanic ultramafic rocks. Earth and Planetary Science Letters, 21, 97–107.

Shaw, D.M. (1995) Lunar behaviour of boron contrasted with the terrestrial boron cycle. Meteoritics, 30, 199–208.

Shaw, D.M., Higgins, M.D., Truscott, M.G., and Middleton, T.A. (1988a) Boron contamination in polished thin sections of meteorites: Implications for other trace-element studies by alpha-track image or ion microprobe. American Mineralogist, 73, 894–900.

Shaw, D.M., Truscott, M.G., Gray, E.A., and Middleton, T.A. (1988b) Boron and lithium in high-grade rocks and minerals from the Wawa-Kapuskasing region, Ontario. Canadian Journal of Earth Science, 25, 1485–1502.

Shearer, C.K., and Papike, J.J. (1986) Distribution of boron in the Tip Top pegmatite, Black Hills, South Dakota. Geology, 14, 119–123.

Truscott, M.G., and Shaw, D.M. (1984) Boron in chert and Precambrian siliceous iron formations. Geochimica et Cosmochimica Acta, 48, 2313–2320.

Truscott, M.G., Shaw, D.M., and Cramer, J.J. (1986) Boron abundance and localization in granulites and the lower continental crust. Bulletin of the Geological Society of Finland, 58(1), 169–177.

Werding, G., and Schreyer, W. (1984) Alkali-free tourmaline in the system MgO-Al₂O₃-B₂O₃-SiO₂-H₂O. Geochimica et Cosmochimica Acta, 48, 1331–1344.